IEEE Access
Multidisciplinary ⋮ Rapid Review ⋮ Open Access Journal

Received December 31, 2019, accepted January 12, 2020, date of publication January 15, 2020, date of current version January 27, 2020.

Digital Object Identifier 10.1109/ACCESS.2020.2966786

A Novel Tiered Type Permanent Magnet Spherical Motor and Its Rotor Orientation Measurement Principle

FENG CHAI, (Member, IEEE), LEI GAN, AND LEI CHEN
Department of Electrical Engineering, Harbin Institute of Technology, Harbin 150080, China

Corresponding author: Lei Chen (hitchenlei@hit.edu.cn)

This work was supported by the National Natural Science Foundation of China under Grant 51477032 and Grant 51677039.

ABSTRACT This paper proposes a novel tiered type permanent magnet spherical motor (T-PMSpM), which has the advantage of relatively larger torque ability compared with most existing spherical motors. The proposed T-PMSpM is capable of continuously rotating while the rotating shaft can tilt in all directions. Considering that it is usually much difficult to measure the multi-DOF rotor orientation of a spherical motor in an easy and convenient way, this paper also proposes a specific rotor orientation measurement method, aiming at providing an idea of simple solution for detecting the multi-DOF rotor orientation based on phase difference. In order to clearly reveal the intrinsic relationship between the phenomenon of phase shift and the tilting motion, a simplified back-EMF model of the T-PMSpM is put forward according to the geometric changes as the rotor tilts. Based on the simplified back-EMF model, both the initial phase and the magnitude of the back-EMF are calculated analytically and verified by the 3D FEM. The full region forward relationship between the rotor tilting position and the phase difference is further obtained. Therefore, the rotor tilting position can be easily identified based on the inverse solution. Finally, a prototype motor of the investigated T-PMSpM has been manufactured. The experimental results validate that the multi-DOF orientation can be detected effectively with enough accuracy.

INDEX TERMS Spherical motor, multi-degree-of-freedom (multi-DOF), orientation measurement method, permanent magnet (PM), back-electromagnetic force (back-EMF).

I. INTRODUCTION

Spherical motors are gaining increasing popularity in robotics and industrial applications in recent years. Today, a variety of spherical motors have been designed and studied [1]–[4]. Among them, the tiered type permanent magnet spherical motors (T-PMSpMs) have gradually become a research hotspot for their simplicity in both structures and control principles [5]–[8]. They usually have more than one layer of stators along axial direction, each layer consists of a circle of evenly distributed coils. Different from other spherical motors, the T-PMSpMs are asymmetric in the three directions, i.e., the output shaft can rotate continuously but only tilt in a limited range. Thus, the T-PMSpMs are more suitable for wheels, propellers, and machine tools that require orientation control of the rotating shaft [9].

The associate editor coordinating the review of this manuscript and approving it for publication was Di He.

However, in order to create a linear torque characteristic so that the design, calculation and control could become relatively simple, most of the T-PMSpMs do not have iron cores. As a result, it is hard for them to produce a powerful output torque. In [10], a permanent magnet (PM) spherical motor, of which the rated torque is 0.80 N·m when rotor diameter is 114 mm, has been proposed. The corresponding torque density, which is defined as the torque per unit volume of rotor sphere, is about 1.03 N·m/L. In [11], an iron shell is employed in the PM spherical motor to increase the torque ability and a higher torque density of about 1.28 N·m/L is achieved. Despite that the use of iron shell can enhance the torque ability effectively [12], the torque density is still too low due to the large air gap caused by use of air-cored coils.

The multi-DOF rotor orientation measurement is very important for spherical motors. However, compared with conventional single-DOF rotary motors, the T-PMSpMs have more than one degree of freedom, i.e., both the rotation

and tilting positions are required, which makes it difficult to measure the rotor orientation by simply using a single sensor such as a rotary encoder or a resolver [13]. To solve this problem, many orientation measurement methods for detecting multi-DOF motions have been proposed [14]–[16]. According to their working principles, the existing orientation measurement methods used in spherical motors can be generally divided into three groups, i.e., the mechanical frame based method, the optical based method and the magnetic field based method.

The mechanical frame based method, which simply uses three single-axis encoders to measure the three independent position angles mechanically decoupled by the gimbal, is a typical contact method. Lee *et al*. proposed the concept of a spherical stepper motor, of which the rotor orientation was measured based on three circular guides that are perpendicular to each other [17]. Although this method has the merit of high resolution, the influence of the additional mechanical linkage on the motion characteristic is non-negligible [18], [19]. To minimize the negative influence of the measurement system, including the introduced inertia and friction, Zhang *et al*. developed a special spherical joint that contains an encoder and a two-axis tilt sensor to measure the rotor orientation [20]. This spherical joint is also served as a multi-DOF bearing that supports the rotor by being installed in the center of the rotor.

The optical based method has two development branches. One is based on the light sensors and binary painting, where only two colors, i.e., black and white, are painted with specific patterns on the rotor surface [21], [22]. The other is based on the vision sensors, which usually requires elaborate grids or color patterns [15], [23]. In some cases, even no engineered pattern is needed. Lee and Zhou proposed dual-sensor system to detect the incremental three-DOF motions of a spherical wrist actuator based on the natural microscope features, which was inspired by the working principle of the optical mouse [24]. However, most optical based methods have some limitations when they are adopted in a fast dynamic system, since their sampling rate is relatively low [25].

The magnetic field based method takes full advantage of the magnetic field distribution of the PM rotor, based on the fact that most magnetic field models are position-dependent [26]. In this method, several magnetic field sensors, such as Hall-effect sensors, are deployed around the rotor [27]–[29]. Wang *et al*. proposed a PM spherical actuator, of which the rotor orientation was deduced by using four or six sensors [30], [31]. It is worth noting that the magnetic field based method requires a complete knowledge of the magnetic field distribution, thus many magnetic field calculation methods are proposed to deal with different magnetic situations [32]–[35]. However, the magnetic field calculation will become much difficult when massive iron cores are applied in order to enhance the torque ability.

As an alternative idea, the magnetic field of an external PM rather than the PM rotor is utilized. Li *et al*. proposed a 3-DOF deflection type PM motor, with a regular PM installed on the top of the rotor output shaft [16]. This method can avoid complicated calculation of rotor magnetic field. Nevertheless, the orientation detection methods based on the direct measurement of magnetic field still have the problem of relatively low resolution, considering that the magnetic field of PM rotor or external PM does not change much at certain positions [36].

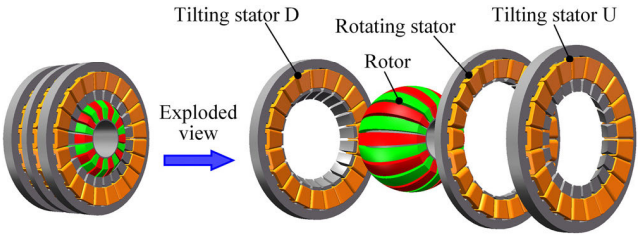

FIGURE 1. Basic structure of the investigated T-PMSpM.

The magnetic field of the PM rotor can also be utilized indirectly. In fact, the sensor-less rotor orientation measurement method based on back-EMF is widely used in single-DOF PM synchronous motors already [37], [38]. Similarly, the rotor orientation detection method based on back-EMF can also be extended and adopted in spherical motor applications. Bai *et al*. proposed a back-EMF method for sensing the real-time multi-DOF motion of a PM spherical motor, of which the structural simplicity was retained since no sensors were installed [13]. However, it is noticed that a magnetic flux model is required to characterize the relationship between the induced voltage and the magnetic flux change, which is actually hard to be obtained in an iron-cored tiered type spherical motor.

In this paper, on the one hand, a novel iron-cored tiered type permanent magnet spherical motor with the merit of large torque ability is proposed. The basic structure and working principle are presented in detail. On the other hand, a multi-DOF rotor orientation measurement method based on phase difference is proposed. It can avoid complex calculation of magnetic field distribution in spherical motors. The principle of rotor orientation measurement is explained and also verified by the FEM and experiments.

II. BASIC STRUCTURE AND WORKING PRINCIPLE OF THE INVESTIGATED T-PMSPM

The basic structure of the investigated iron-cored T-PMSpM is shown in Fig. 1. The spherical rotor makes it possible to achieve 3-DOF motions. Common rotor configurations in PM synchronous motors, such as surface-mounted and spoke PM type, can also be transplanted here. There are three stators along axial direction. The middle rotating stator, as the name implies, is designed to generate the rotating motion, whereas the two tilting stators are used to generate the tilting motion. Specially, the iron cores are adopted in the stators to enhance the torque ability.

For the rotating motion, the T-PMSpM has the same working principle as that of the PM synchronous motors, i.e., a rotating torque T_q is exerted on the rotor by the middle

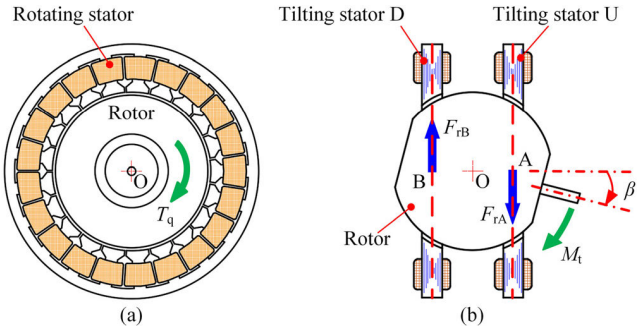

FIGURE 2. Demonstration of (a) rotating and (b) tilting motions.

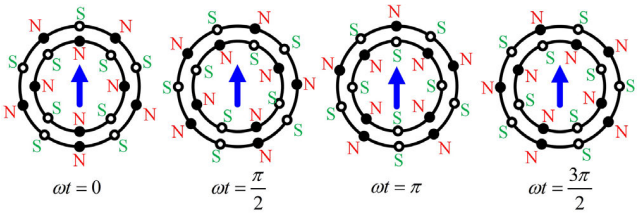

FIGURE 3. Demonstration of the constant electromagnetic force.

rotating stator as illustrated in Fig. 2(a), where the tilting stators are not shown for a clear view. For the tilting motion, a constant tilting torque of the electromagnetic force couple M_t is produced to tilt the rotor as illustrated in Fig. 2(b).

The rotating stator is not shown in Fig. 2(b) since the tilting motion is only decided by the two tilting stators. It can be observed that the tilting torque M_t consists of two non-collinear electromagnetic forces F_{rA} and F_{rB}, which are equal in magnitude but opposite in direction. In fact, these two constant electromagnetic forces are produced based on the theory of self-bearing motors [39]. As shown in Fig. 3, the relationship between the constant electromagnetic force and the air gap magnetic field is demonstrated.

In Fig. 3, the inner circle represents for the rotor magnetic field with 8 magnetic poles while the outer circle represents for the stator magnetic field with 10 magnetic poles. It is noticed that the stator magnetic field has exactly 2 more magnetic poles than that of the rotor magnetic field. Thus when the rotor revolves with electrical radian frequency ω, a constant upward electromagnetic force will be produced as long as the stator magnetic field also rotates in the same direction with the same electrical radian frequency.

Now, it can be concluded from the working principle that the rotating motion and tilting motion can be controlled by different stators respectively.

Main specifications of the investigated T-PMSpM is given in Table 1.

A relatively high torque density of about 31.84 N·m/L can be achieved by the investigated iron-cored T-PMSpM, where the pole-slot combination of 20 poles and 21 slots is adopted. More details about the torque performances and magnetic field features can be found in [40], [41].

TABLE 1. Main specifications of the investigated T-PMSpM.

Parameter	Value	Unit
Stator outer diameter (cylindrical)	250	mm
Rotor outer diameter (spherical)	156	mm
Stack length of the rotating stator	12	mm
Axial position of the rotating stator	[-6, 6]	mm
Stack length of the tilting stator	20	mm
Axial position of the tilting stator	[-50, -30], [30, 50]	mm
Rotor axial length	120	mm
Rated rotating speed	500	rpm
Rated rotating torque	63.3	N·m
Rated torque density	31.84	N·m/L

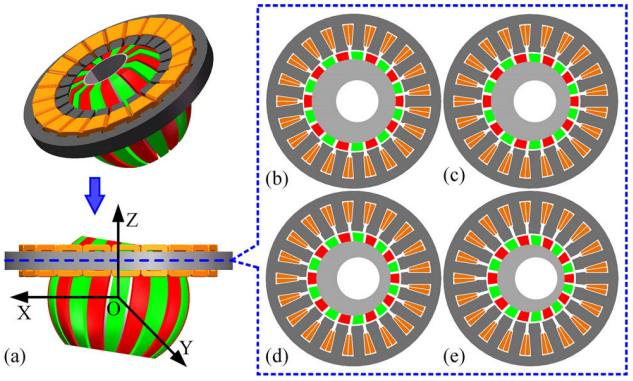

FIGURE 4. Tilting stator and rotor. (a) 3D model. (b)–(e) Cross sections in different axial positions with z = 32.5 mm, z = 37.5 mm, z = 42.5 mm and z = 47.5 mm, respectively, when tilting angle $\beta = 9°$.

III. SIMPLIFIED BACK-EMF MODEL

In this paper, the rotor orientation is measured based on the phase information that contained in the back-EMF. Therefore, the back-EMF of the proposed T-PMSpM is investigated at first. Considering that the 3D FEM is too time-consuming, a simplified back-EMF model of the T-PMSpM is proposed for fast calculation. In fact, the simplified back-EMF model also helps to understand the intrinsic relationship between the rotor orientation and the back-EMF.

A. BACK-EMF IN THE TILTING STATOR

The back-EMF in the tilting stator is calculated based on the 2D cross sections, but with the tilting motion taken into account, as demonstrated in Fig. 4. It can be observed that the shape and dimensions of the rotor PMs and iron core are changed after the rotor tilts. In particular, the circumferential angular positions as well as the widths of the PMs in the cross-sectional plane are also changed, i.e., the PMs are no longer evenly distributed.

Besides, it is noticed that the cross sections are slightly different from each other, as their axial positions vary from the nearest to the farthest distance to the motor center. In order to take into account the 3D spherical structure, the axial segmentation calculation method is applied, i.e., the tilting stator is divided into several slices along axial direction. If these slices are thin enough, the axial changes in one slice

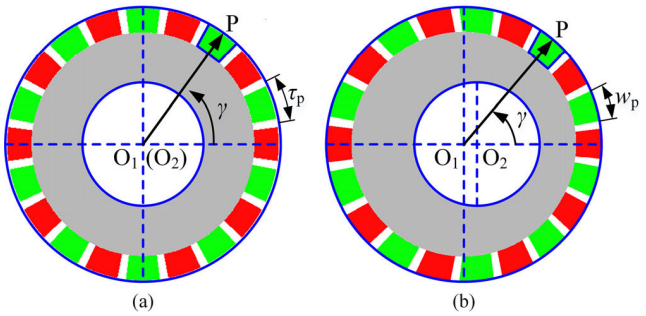

FIGURE 5. Rotor cross section. (a) Before rotor tilts. (b) After rotor tilts.

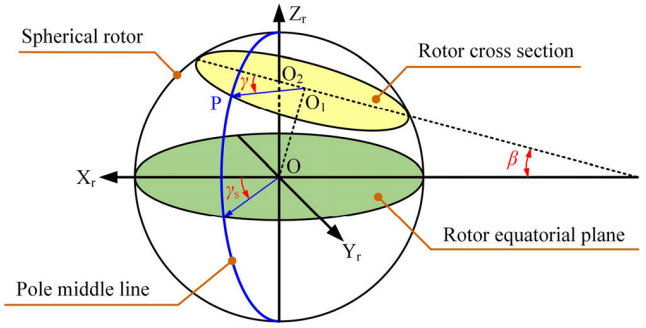

FIGURE 6. Relationship between the two angles γ and γ_S.

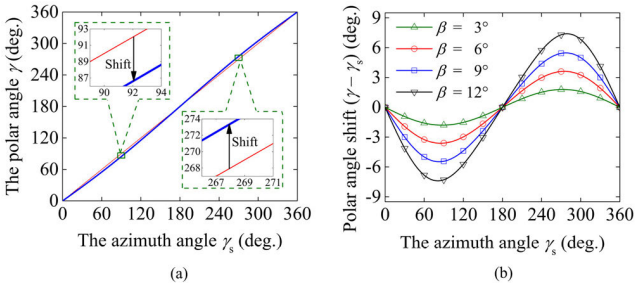

FIGURE 7. Angular position of rotor pole. (a) Curve of polar angle γ when tilting angle $\beta = 9°$. (b) Curves of $(\gamma - \gamma_S)$ with various tilting angles.

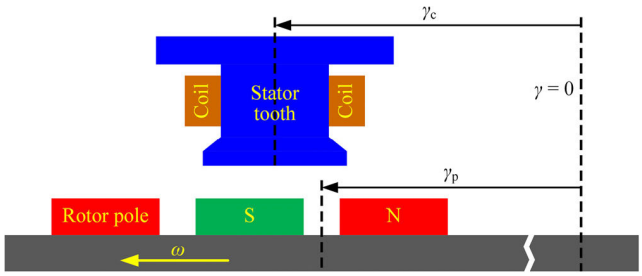

FIGURE 8. Demonstration for the initial phase calculation.

can be neglected, which means that they can be calculated in 2D and further represented by their middle cross sections. In fact, the stator slots are designed to be identical along axial direction, thus the stator in cross sections looks very similar.

For any of the above middle cross sections, it is very important to obtain the circumferential angular positions of the PMs after the rotor tilts, so that the tilting motion can be fully considered in the simplified back-EMF model.

As shown in Fig. 5, point O_1 is the center of the rotor cross section, and point O_2 is the center of the hollow shaft in the cross section. The circumferential angular position (point P) is measured using the polar angle γ in the polar coordinate system, which is located in the cross-sectional plane. The relationship between this polar angle γ and the corresponding azimuth angle γ_s in the rotor spherical coordinate system is shown in Fig. 6, where the tilting angle is denoted as β. The pole middle line is a longitude line through point P.

By applying the knowledge of solid geometry, the relationship between γ and γ_s is obtained analytically as

$$\gamma = \pi/2 + \arcsin \frac{\sin\zeta \cdot \left[\frac{\tan\gamma_s}{\sin\beta} - \frac{1}{\tan\beta\tan\zeta}\right] \cdot l_x}{\sqrt{R_R^2 - l_x^2}} - \zeta \quad (1)$$

where R_R is the outer radius of the spherical rotor, l_x is the distance between the rotor cross section and the center of the rotor, and $\zeta = \arccos\{\cos\{\arctan[\cos\gamma_s \tan\beta]\} \cdot \sin\gamma_s\}$.

When the rotor tilts to a certain tilting angle, the curve of the circumferential angular position is given in Fig. 7(a). It can be observed that the polar angle γ is not equal to the azimuth angle γ_s due to the tilting motion. As a matter of fact, there is an angle shift denoted by $(\gamma - \gamma_s)$ between them, as illustrated in Fig. 7(b). It is worth noting that the angle shift will be multiplied by the number of pole-pairs p in the phase shift of the back-EMF since the phase shift is expressed by electric degree. Similarly, the full region mapping relationship $\gamma = f_a(\beta, \gamma_s)$ can be obtained with arbitrary tilting angle β according on (1).

Thus, as demonstrated in Fig. 8, the initial phase of a tooth coil's induced voltage can be calculated as

$$\psi_{c\_i,j} = p \cdot \left[f_a^{-1}(\beta, \gamma_{p\_i,j}) - f_a^{-1}(\beta, \gamma_{c\_i,j})\right] \quad (2)$$

where γ_c and γ_p are the polar angles of a coil and a magnetic neutral plane, respectively. The subscript i and j are the sequence numbers of the slice and the tooth, respectively.

Considering that the phase information is the priority for orientation measurement, the relative magnitude rather than the absolute magnitude is calculated for further simplification. The relative magnitude of the back-EMF is calculated based on the relative pole-arc coefficient α_{pr}, which is defined as

$$\alpha_{pr} = w_p/\tau_p \quad (3)$$

where w_p is the width of the rotor pole in rotor cross section, and τ_p is pole pitch before the rotor tilts as shown in Fig. 5.

By applying the knowledge of solid geometry, the relative pole-arc coefficient α_{pr} can be obtained, as shown in Fig. 9.

Based on the fact that the rotor magnetic field distribution in the air gap is almost sinusoidal along circumferential direction after rotor pole optimization, only the fundamental component of rotor magnetic field needs to be considered.

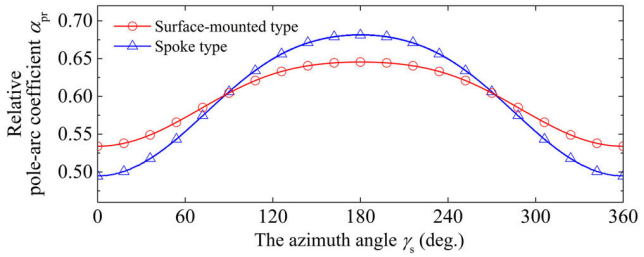

FIGURE 9. Relative pole-arc coefficient when tilting angle $\beta = 9°$.

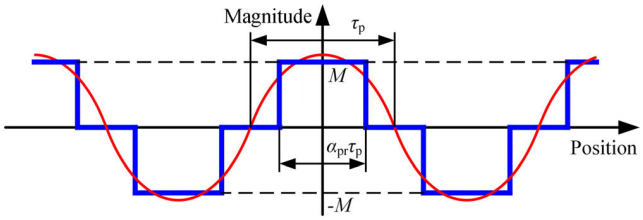

FIGURE 10. Fundamental component of the three-level square wave.

According to the Fourier series of a three-level square wave as shown in Fig. 10, the magnitude of the fundamental component is obtained as

$$A_1 = \frac{4}{\pi} M \cdot \sin\left(\frac{\pi}{2}\alpha_{\mathrm{pr}}\right) \tag{4}$$

It can be found out from (4) that the magnitude of the fundamental component is proportional to the sine of the product of $\pi/2$ and the pole-arc coefficient α_{pr}. Therefore, the magnitude of a coil's induced voltage can be expressed as

$$E_{\mathrm{c\_}i,j} = C_{\mathrm{m}} \cdot \sin\left[\frac{\pi}{2}\alpha_{\mathrm{pr}}\left(\beta, \gamma_{\mathrm{s\_}i,j}\right)\right] \tag{5}$$

where C_{m} is a constant coefficient, α_{pr} is the function of the tilting angle β and the azimuth angle $\gamma_{\mathrm{s\_i,j}}$.

As the rotor revolves, the fundamental component of a tooth coil's induced voltage can be expressed as

$$e(t)_{\mathrm{c\_}i,j} = E_{\mathrm{c\_}i,j}\cos\left(\omega t + \psi_{\mathrm{c\_}i,j}\right) \tag{6}$$

Finally, the phase back-EMF $e(t)_{\mathrm{p}}$ can be calculated by the sum of the coil's induced voltages $e(t)_{\mathrm{c\_i,j}}$ as

$$e(t)_{\mathrm{p}} = \sum_{i=1}^{N_{\mathrm{S}}}\sum_{j=1}^{N_{\mathrm{P}}} e(t)_{\mathrm{c\_}i,j} \tag{7}$$

where N_{S} is the number of axial segments of the tilting stator, and N_{P} is the number of coils in one phase.

The coil's induced voltage and the phase back-EMF can be expressed by the phasor as

$$\dot{E}_{\mathrm{c\_}i,j} = E_{\mathrm{c\_}i,j}e^{j\psi_{\mathrm{c\_}i,j}} = E_{\mathrm{c\_}i,j}\angle\psi_{\mathrm{c\_}i,j} \tag{8}$$

$$\dot{E}_{\mathrm{p}} = E_{\mathrm{p}}e^{j\psi_{\mathrm{p}}} = E_{\mathrm{p}}\angle\psi_{\mathrm{p}} = \sum_{i=1}^{N_{\mathrm{S}}}\sum_{j=1}^{N_{\mathrm{P}}}\dot{E}_{\mathrm{c\_}i,j} \tag{9}$$

Thus we can obtain both the magnitude and initial phase as

$$\begin{cases} E_{\mathrm{p}} = \sum\limits_{i=1}^{N_{\mathrm{S}}}\sum\limits_{j=1}^{N_{\mathrm{P}}} E_{\mathrm{c\_}i,j}\cos\left(\psi_{\mathrm{c\_}i,j}\right) \\ \psi_{\mathrm{p}} = \arctan\left[\dfrac{\sum\limits_{i=1}^{N_{\mathrm{S}}}\sum\limits_{j=1}^{N_{\mathrm{P}}} E_{\mathrm{c\_}i,j}\sin\left(\psi_{\mathrm{c\_}i,j}\right)}{\sum\limits_{i=1}^{N_{\mathrm{S}}}\sum\limits_{j=1}^{N_{\mathrm{P}}} E_{\mathrm{c\_}i,j}\cos\left(\psi_{\mathrm{c\_}i,j}\right)}\right] \end{cases} \tag{10}$$

B. BACK-EMF IN THE ROTATING STATOR

Similarly, the back-EMF in the rotating stator can also be obtained by using the cross sections as shown in Fig. 11.

It can be observed that the tilting motion has little influence on the above cross section. In fact, the polar angle γ is almost equal to the azimuth angle γ_{s} as shown in Fig. 12(a). As a result, the polar angle shift (γ–γ_{s}) is very small as shown in Fig. 12(b). Therefore, it can be assumed that the tilting motion has little influence on the back-EMF in the rotating stator. This assumption is also verified by the 3D FEM results as shown in Fig. 13, where the curves of back-EMF with different tilting angle β do not change much.

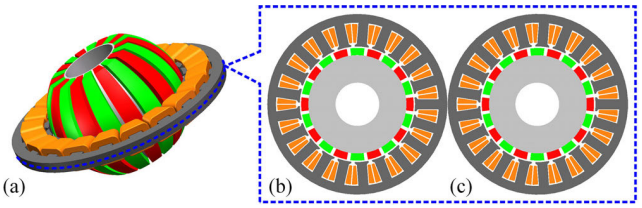

FIGURE 11. Rotating stator and rotor. (a) 3D model. (b) Cross section with z = 0 mm, $\beta = 9°$. (c) Cross section with z = 5.5 mm, $\beta = 9°$.

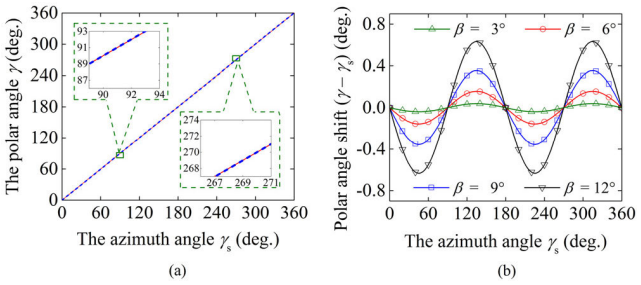

FIGURE 12. Angular position of rotor pole. (a) Curve of polar angle γ when tilting angle $\beta = 9°$. (b) Curves of ($\gamma - \gamma_s$) with various tilting angles.

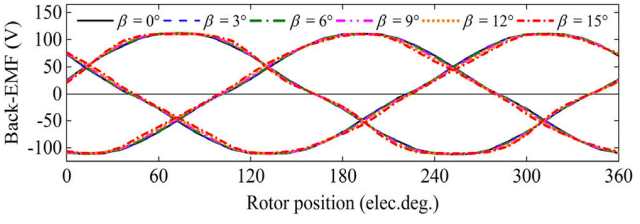

FIGURE 13. Back-EMF in the rotating stator calculated by 3D FEM.

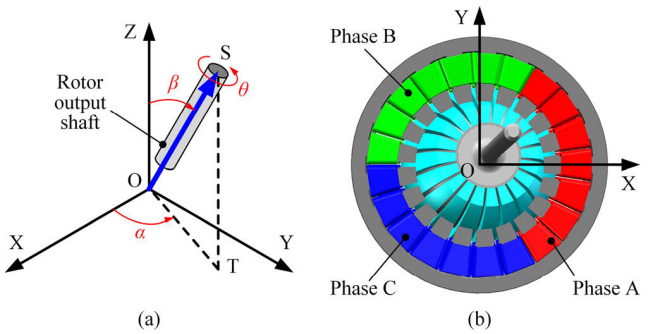

FIGURE 14. Definition of the rotor position angles. (a) Rotor output shaft. (b) Relative position of the three-phase winding.

Based on the above facts, the rotating stator can be used to detect the rotating motion, rather than detect the tilting motion. In this case, the common back-EMF methods used in single-DOF PM synchronous motors can be directly adopted.

IV. ORIENTATION DETECTION BASED ON BACK-EMF

A. POSITION ANGLE DEFINITION

The tilting motion can be generally defined by two angles, i.e., the azimuth angle α that indicates the tilting direction and the zenith angle β that indicates the tilting angle in the stator spherical coordinate system, as shown in Fig. 14(a).

Meanwhile, the rotating motion is defined by the rotating angle θ of the rotor around its own output shaft. Besides, the relative position relationship between the stator spherical coordinate system and the three-phase windings are shown in Fig. 14(b). The X-axis is placed in the central axis of phase A.

B. BACK-EMF ANALYSIS

The initial phase and relative magnitude of the back-EMF are obtained using the proposed simplified back-EMF model, with the tilting motion taken into account. The results of the initial phase are shown in Fig. 15, where the tilting stator is segmented into 10 slices with a small thickness of 2 mm.

The results of a single slice in different axial positions are shown in Fig. 15(a)–(c). It can be observed that the slice with the axial position $z = 31$ mm, which is the closest slice to the motor center, has a smaller phase shift than the FEM results, whereas the slice with the farthest axial position $z = 49$ mm has a larger phase shift than the FEM results, as the rotor tilts. As a consequence, the result of the stator slice with the axial position $z = 38$ mm matches the FEM results best. However, this special axial position is difficult to be predicted before the calculation. Therefore, the synthetic result that calculated from all the stator slices is adopted to evaluate the initial phase of the back-EMF as shown in Fig. 15(d). It can be observed that the synthetic result is in good agreement with the 3D FEM results as the tilting angle varies.

The relative magnitude of the back-EMF is also obtained synthetically. In order to compare with the 3D FEM results,

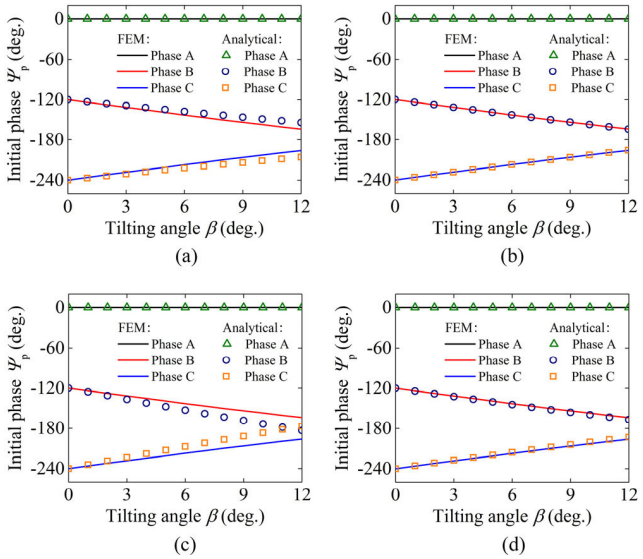

FIGURE 15. Results of the Initial phase. (a)–(c) From a single slice in different axial positions with z = 31 mm, z = 38 mm and z = 49 mm, respectively. (d) Synthetic result of all slices.

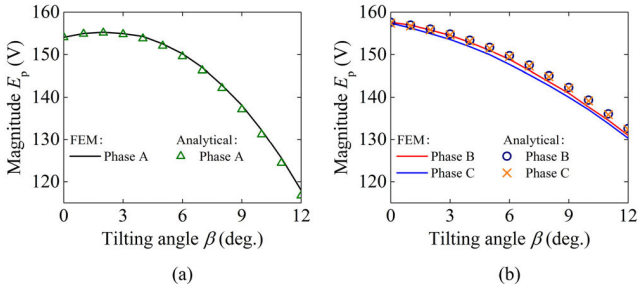

FIGURE 16. Results of the magnitude. (a) From phase A. (b) From phase B and C.

the constant coefficient C_{m} is selected as

$$C_{\mathrm{m}} = E_{\mathrm{FEM},\beta=0^\circ} \big/ E_{\mathrm{p},\beta=0^\circ} \tag{11}$$

where E_{FEM}, $\beta = 0^\circ$ and $E_{\mathrm{p}}, \beta = 0^\circ$ are the magnitudes from the 3D FEM and the proposed back-EMF model, respectively.

In this case, the results of the magnitude are illustrated in Fig. 16. It can be observed that the analytical and the FEM results have the same trends as the tilting angle increases.

Compared with the curves of magnitude in Fig. 16, it is obvious that the curves of initial phase in Fig. 15 have better linearity and monotonicity. Therefore, the initial phase of the back-EMF is more suitable in rotor orientation measurement.

The above results are obtained in tilting direction $\alpha = 0^\circ$. In fact, both the tilting angle β and the tilting direction α can be obtained based on the phase differences $\Psi_{\mathrm{pAB}} = \Psi_{\mathrm{pA}} - \Psi_{\mathrm{pB}}$ and $\Psi_{\mathrm{pBC}} = \Psi_{\mathrm{pB}} - \Psi_{\mathrm{pC}}$. Here, the phase difference is adopted because it can describe the relative change of the initial phase better. When the rotor tilts in different tilting directions, the relationships between the phase differences and the tilting angle are shown in Fig. 17.

It can be observed from Fig. 17 that the phase difference is almost linear with the tilting angle. Besides, the variation

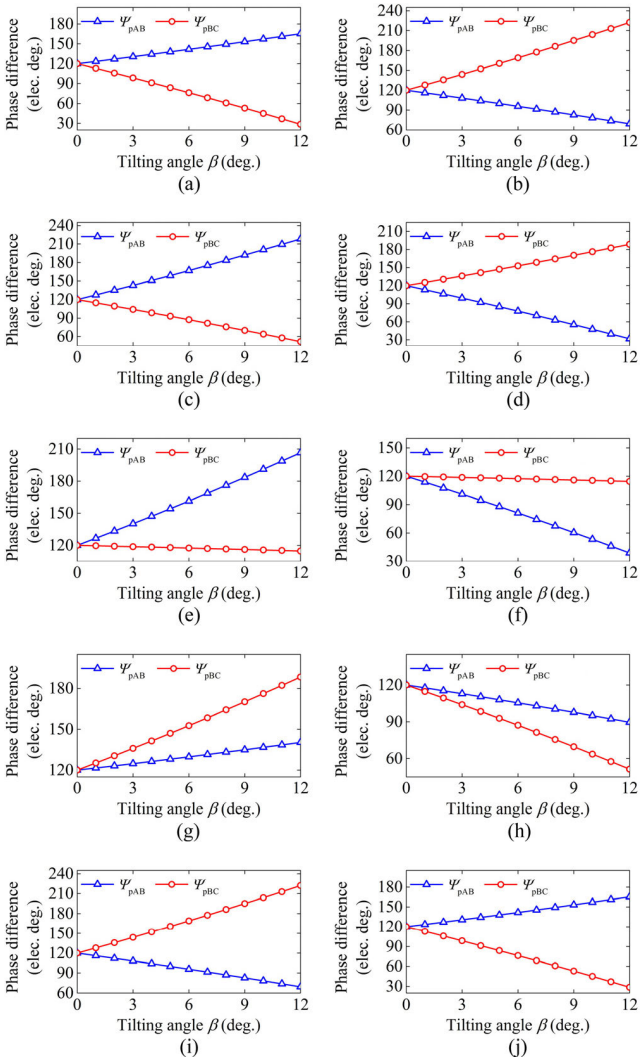

FIGURE 17. Phase difference of the back-EMF in tilting stators. (a) Tilting stator U with $\alpha = 0°$. (b) Tilting stator D with $\alpha = 0°$. (c) Tilting stator U with $\alpha = 45°$. (d) Tilting stator D with $\alpha = 45°$. (e) Tilting stator U with $\alpha = 90°$. (f) Tilting stator D with $\alpha = 90°$. (g) Tilting stator U with $\alpha = 135°$. (h) Tilting stator D with $\alpha = 135°$. (i) Tilting stator U with $\alpha = 180°$. (j) Tilting stator D with $\alpha = 180°$.

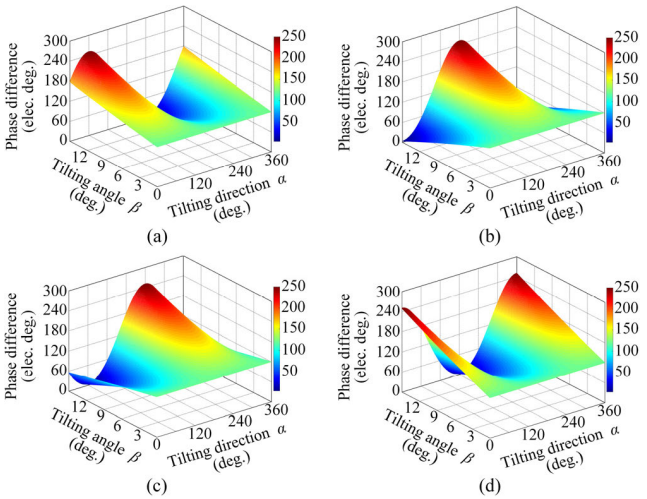

FIGURE 18. Phase difference of the back-EMF varies with tilting direction α and tilting angle β. (a) Phase difference Ψ_{pAB} from tilting stator U. (b) Phase difference Ψ_{pBC} from tilting stator U. (c) Phase difference Ψ_{pAB} from tilting stator D. (d) Phase difference Ψ_{pBC} from tilting stator D.

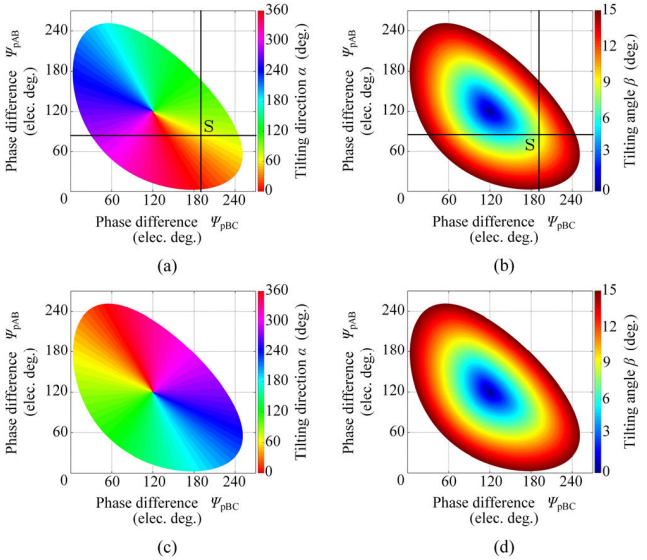

FIGURE 19. Results of the inverse solution. (a) Tilting direction α detected by tilting stator U. (b) Tilting angle β detected by tilting stator U. (c) Tilting direction α detected by tilting stator D. (d) Tilting angle β detected by tilting stator D.

trend obviously changes with the tilting direction. In fact, it can be proved that there only exists one unique combination of phase differences Ψ_{pAB} and Ψ_{pBC} that corresponds to a specific tilting position, which is defined by a combination of tilting direction α and tilting angle β.

The full region relationships between the phase differences and the rotor tilting position are further illustrated in Fig. 18.

It is noticed that there is a shift of 180 electrical degrees between the phase differences from the two tilting stators with respect to the tilting direction α, which is caused by the mirror symmetry deployment of tilting stator U and D. Therefore, any of the two tilting stators can actually be used to detect the tilting motion independently.

Now, the inverse solution can be obtained mathematically based on the above full region relationships as illustrated in Fig. 19. Thus, by measuring the phase differences of the three-phase back-EMF from any of the two tilting stators, both the tilting direction α and the tilting angle β can be easily obtained using the look-up table of the inverse solution. Take a data point S in Fig. 19 a) and Fig. 19b) for example, the phase differences Ψ_{pAB} and Ψ_{pBC} are 85 and 195 electrical degrees, respectively, then it can be obtained from the inverse solution that the corresponding tilting direction is 60° and the corresponding tilting angle is 9°.

C. DEPLOYMENT OF DETECTING COILS

Considering that there are situations when the original stator coils or windings are not available to provide the back-EMF for rotor orientation detection. For example, when there are

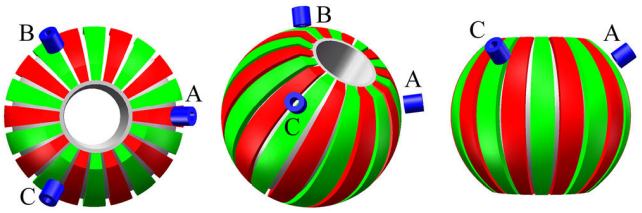

FIGURE 20. Deployment of detecting coils.

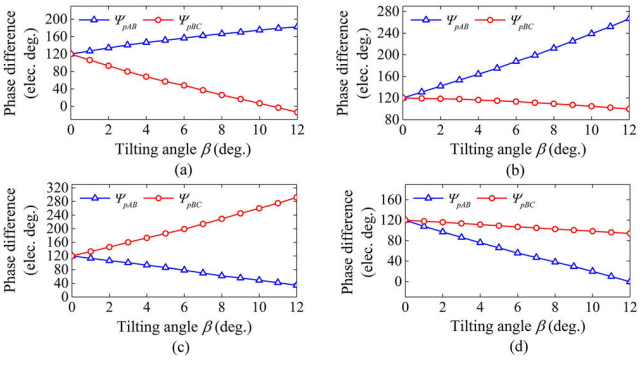

FIGURE 21. Phase difference of the back-EMF in detecting coils. (a) Tilting direction $\alpha = 0°$. (b) Tilting direction $\alpha = 90°$. (c) Tilting direction $\alpha = 180°$. (d) Tilting direction $\alpha = 270°$.

no free phase and it is too time-consuming to extract the back-EMF from the terminal voltage by complex algorithm. In these cases, the rotor orientation detecting coils become an alternative to provide the back-EMF.

Similarly, three detecting coils at least are needed to produce the three-phase back-EMF discussed above. It can be observed from Fig. 20 that the detecting coils are arranged around the PM rotor and evenly distributed in a plane close to the end of the rotor, which is quite similar to the position of the three-phase windings in the tilting stators.

When the rotor tilts in different tilting directions, the relationships between the phase differences and the tilting angle are shown in Fig. 21, of which the variation trend is very similar to that of Fig. 17. Therefore, the detecting coils can also be made full use of to detect the rotor orientation.

V. EXPERIMENTAL VERIFICATION

A. EXPERIMENTAL SETUP

A prototype motor of the investigated T-PMSpM has been manufactured to validate the proposed multi-DOF orientation measurement method. The experimental setup used for back-EMF measurement is illustrated in Fig. 22. The servo motor, together with its pedestal, can move around the prototype motor manually as the tilting angle β varies, as demonstrated in Fig. 22(b) and Fig. 22(c).

In the back-EMF measurement, the prototype motor is driven by the servo motor and rotates at a constant speed. Then, the three-phase back-EMF waveforms from the three stators are measured with different rotor tilting positions, respectively. The arc guide is used to indicate the tilting angle of the output shaft.

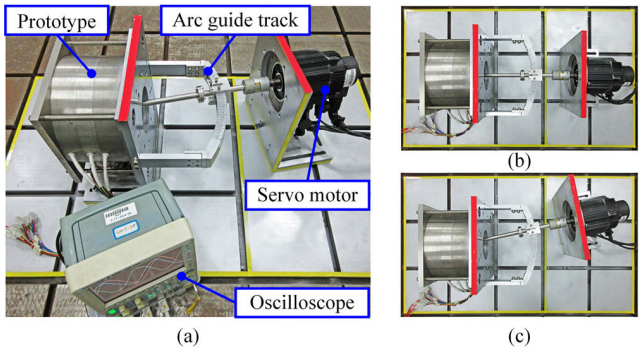

FIGURE 22. Experimental setup. (a) Overall view. (b)–(c) Top view with tilting angle $\beta = 0°$ and $\beta = 12°$, respectively.

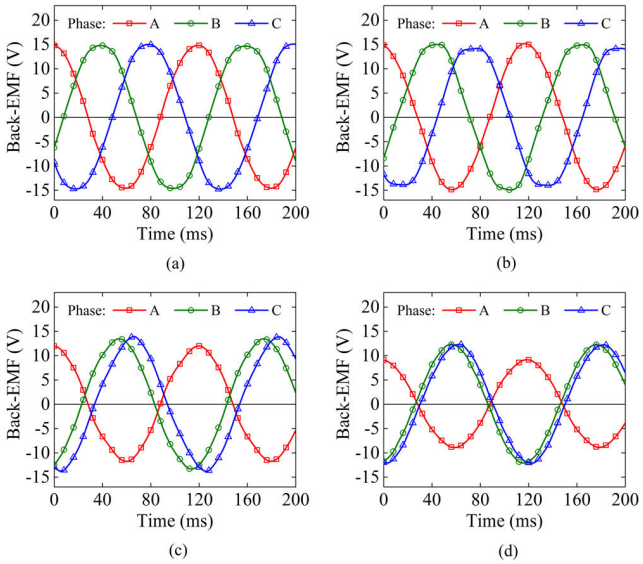

FIGURE 23. Measured phase back-EMF waveform from tilting stator U when the tilting direction $\alpha = 0°$. (a) Tilting angle $\beta = 0°$. (b) Tilting angle $\beta = 3°$. (c) Tilting angle $\beta = 12°$. (d) Tilting angle $\beta = 15°$.

B. MEASURED RESULTS

The back-EMF was measured with a constant rotating speed of 50 rpm. The range of the tilting angle β in the experiments is from 0° to 15° with an increment of 1° when two different tilting directions of 0° and 90° are investigated, respectively.

Some representative results of the measured back-EMF with tilting directions of 0° and 90° are illustrated in Fig. 23 and Fig.24, respectively. It can be observed that, on the one hand, the three-phase symmetry of the back-EMF no longer exists after the rotor tilts, and on the other hand, the variation trends with different tilting directions are also different. In fact, the phase difference changes in the same way exactly as theoretically calculated above when the tilting direction α and tilting angle β vary simultaneously.

Based on the measured results of three-phase back-EMF, the values of phase differences with various rotor orientations can be obtained. Thus the rotor tilting positions, i.e., the tilting direction α and tilting angle β can be easily calculated according to the inverse solution, which is given in Fig. 19.

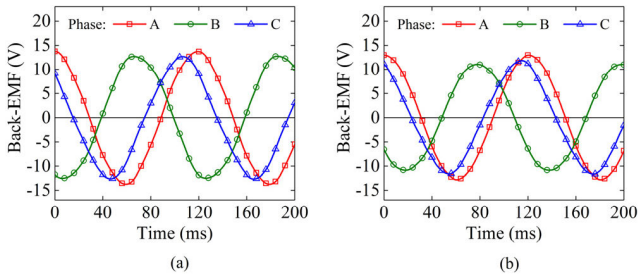

FIGURE 24. Measured phase back-EMF waveform from tilting stator U when the tilting direction $\alpha = 90°$. (a) Tilting angle $\beta = 12°$. (b) Tilting angle $\beta = 15°$.

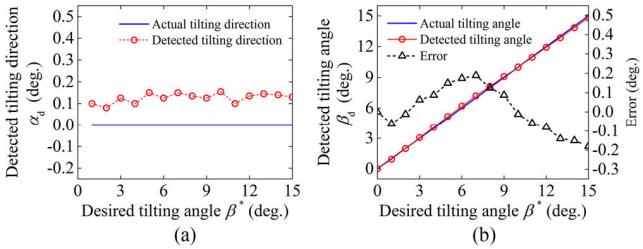

FIGURE 25. Detected rotor tilting positions from tilting stator U when the tilting direction $\alpha = 0°$. (a) Tilting direction. (b) Tilting angle.

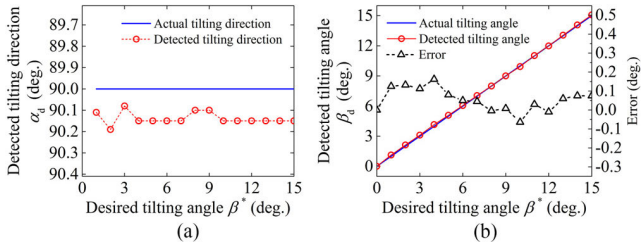

FIGURE 26. Detected rotor tilting positions from tilting stator U when the tilting direction $\alpha = 0°$. (a) Tilting direction. (b) Tilting angle.

The experimentally detected results with tilting directions of 0° are shown in Fig. 25, where the detected results are also compared with the actual values for verification. It can be observed that the detected results are in good agreement with the actual values, the maximum errors of the tilting direction α and the tilting angle β are both smaller than 0.2°.

The experimentally detected results with the other tilting directions of 90° are shown in Fig. 26. It can be observed that the detected results are still in good agreement with the actual values when the rotor tilts in different tilting direction, which validates that not only the tilting angle β but also the tilting direction α can be detected by the back-EMF.

The experiments verify that the proposed multi-DOF orientation measurement method can be utilized to detect the rotor tilting position of the T-PMSpM effectively.

VI. CONCLUSION

In this paper, a novel tiered type permanent magnet spherical motor with the advantage of larger torque ability is proposed. In order to create a simple solution for detecting the multi-DOF rotor orientation, which is critical but also difficult for spherical motors, a multi-DOF rotor orientation measurement method is specially proposed by making full use of the phase difference. On the one hand, the tilting stators or detecting coils are used to detect the tilting motion based on the phase differences of the three-phase back-EMF, which change as the rotor tilts. On the other hand, the rotating stator can be used to detect the rotating motion like common PM synchronous motors, based on the fact that its back-EMF is insensitive to the tilting motion.

From the analytical calculation which is performed by using the simplified back-EMF models, it can be concluded that the intrinsic reason of the phase-shift phenomenon is actually the change of the geometric relationship between the rotor and the stators, especially the change of the positions of the rotor poles. The three-phase symmetry of the back-EMF will no longer exist after the rotor tilts, however, the phase differences of the asymmetric back-EMF contain complete information about the rotor tilting position. Therefore, both the tilting direction and the tilting angle can be easily calculated based on the phase differences according to the inverse solution.

The back-EMF of the prototype is measured with different tilting angles in two different tilting directions for verification. The rotor positions detected from the measured back-EMF are in good agreement with the actual values, thus validating the correctness and effectiveness of the proposed multi-DOF rotor orientation measurement method.

REFERENCES

[1] J. F. P. Fernandes and P. J. C. Branco, "The shell-like spherical induction motor for low-speed traction: Electromagnetic design, analysis, and experimental tests," *IEEE Trans. Ind. Electron.*, vol. 63, no. 7, pp. 4325–4335, Jul. 2016.

[2] H. Son and K.-M. Lee, "Open-loop controller design and dynamic characteristics of a spherical wheel motor," *IEEE Trans. Ind. Electron.*, vol. 57, no. 10, pp. 3475–3482, Oct. 2010.

[3] B. Li, S. Zhang, G. Li, and H. Li, "Synthesis strategy for stator magnetic field of permanent magnet spherical motor," *IEEE Trans. Magn.*, vol. 54, no. 10, Oct. 2018, Art. no. 8203105.

[4] N. Kasashima, K. Ashida, T. Yano, A. Gofuku, and M. Shibata, "Torque control method of an electromagnetic spherical motor using torque map," *IEEE/ASME Trans. Mechatronics*, vol. 21, no. 4, pp. 2050–2060, Aug. 2016.

[5] S. Cho, J.-S. Lim, Y. J. Oh, G. Jeong, D.-W. Kang, and J. Lee, "A study on output characteristics of the spherical multi-DOF motor according to the number of phases and pole pitch angles," *IEEE Trans. Magn.*, vol. 54, no. 11, Nov. 2018, Art. no. 8205005.

[6] K. Bai, R. Xu, K.-M. Lee, W. Dai, and Y. Huang, "Design and development of a spherical motor for conformal printing of curved electronics," *IEEE Trans. Ind. Electron.*, vol. 65, no. 11, pp. 9190–9200, Nov. 2018.

[7] C. Xia, C. Guo, and T. Shi, "A neural-network-identifier and fuzzy-controller-based algorithm for dynamic decoupling control of permanent-magnet spherical motor," *IEEE Trans. Ind. Electron.*, vol. 57, no. 8, pp. 2868–2878, Aug. 2010.

[8] S. Ikejiri, K. Hirata, and S. Maeda, "Proposal of electromagnetic spherical actuator with 3-DOF," *COMPEL*, vol. 29, no. 4, pp. 994–1003, Jan. 2010.

[9] K.-M. Lee, H. Son, and J. Joni, "Concept development and design of a spherical wheel motor (SWM)," in *Proc. IEEE Int. Conf. Robot. Autom.*, Apr. 2005, pp. 3652–3657.

[10] L. Zhang, W. Chen, J. Liu, and X. Wu, "Geometric parameter identification for spherical actuator calibration based on torque formula," in *Proc. IEEE Int. Conf. Robot. Autom.*, May 2013, pp. 3666–3671.

[11] H.-J. Lee, H.-J. Park, S.-H. Won, G.-H. Ryu, and J. Lee, "Improvements of performance of multi-DOF spherical motor by double air-gap feature," *J. Elect. Eng. Technol.*, vol. 8, no. 1, pp. 90–96, Jan. 2013.

[12] G. Jinjun, D.-H. Kim, and H. Son, "Effects of magnetic pole design on orientation torque for a spherical motor," *IEEE/ASME Trans. Mechatronics*, vol. 18, no. 4, pp. 1420–1425, Aug. 2013.
[13] K. Bai, K.-M. Lee, and J. Lu, "A magnetic flux model based method for detecting multi-DOF motion of a permanent magnet spherical motor," *Mechatronics*, vol. 39, pp. 217–225, Nov. 2016.
[14] S. Maeda, K. Hirata, and N. Niguchi, "Characteristics verification of an independently controllable electromagnetic spherical motor," *Sensors*, vol. 14, no. 6, pp. 10072–10080, Jun. 2014.
[15] Z. Qian, Q. Wang, L. Ju, A. Wang, and J. Liu, "Studies on vision based absolute orientation detection method of spherical motor," in *Proc. Int. Conf. Electr. Mach. Syst.*, Nov. 2009, Art. no. 11084546.
[16] Z. Li, C. Wang, M. Guo, and J. Ma, "A novel 3-DOF sensing methodology for M-DOF PM motors," in *Proc. IEEE Transp. Electrific. Conf. Expo (ITEC)*, Jun. 2014, Art. no. 15129418.
[17] K.-M. Lee and C.-K. Kwan, "Design concept development of a spherical stepper for robotic applications," *IEEE Trans. Robot. Autom.*, vol. 7, no. 1, pp. 175–181, Feb. 1991.
[18] K. Takahara, K. Hirata, N. Niguchi, Y. Nishiura, and Y. Sakaidani, "Experimental evaluation of the static characteristics of multi-degree-of-freedom spherical actuators," *IEEE Trans. Magn.*, vol. 53, no. 11, Nov. 2017, Art. no. 8205705.
[19] Y.-H. Hwang, S.-R. Kang, S.-W. Cha, and S.-B. Choi, "An electrorheological spherical joint actuator for a haptic master with application to robot-assisted cutting surgery," *Sens. Actuators A, Phys.*, vol. 249, pp. 163–171, Oct. 2016.
[20] L. Zhang, W. Chen, J. Liu, and C. Wen, "A robust adaptive iterative learning control for trajectory tracking of permanent-magnet spherical actuator," *IEEE Trans. Ind. Electron.*, vol. 63, no. 1, pp. 291–301, Jan. 2016.
[21] D. Stein, E. Scheinerman, and G. Chirikjian, "Mathematical models of binary spherical-motion encoders," *IEEE/ASME Trans. Mechatronics*, vol. 8, no. 2, pp. 234–244, Jun. 2003.
[22] J. Xin, C. Xia, H. Li, and T. Shi, "A novel orientation measurement using optical sensor for spherical motor," *Sci. China Technol. Sci.*, vol. 56, no. 6, pp. 1330–1339, Jun. 2013.
[23] Z. Li, "Robust control of PM spherical stepper motor based on neural networks," *IEEE Trans. Ind. Electron.*, vol. 56, no. 8, pp. 2945–2954, Aug. 2009.
[24] K.-M. Lee and D. Zhou, "A spherical encoder for real-time measurements of three-DOF wrist orientations," in *Proc. IEEE/RSJ Int. Conf. Intell. Robots Syst. (IROS)*, Mar. 2004, pp. 1596–1601.
[25] F. Wu, S. Moon, and H. Son, "Orientation measurement based on magnetic inductance by the extended distributed multi-pole model," *Sensors*, vol. 14, no. 7, pp. 11504–11521, Jun. 2014.
[26] S. Foong, K.-M. Lee, and K. Bai, "Harnessing embedded magnetic fields for angular sensing with nanodegree accuracy," *IEEE/ASME Trans. Mechatronics*, vol. 17, no. 4, pp. 687–696, Aug. 2012.
[27] B. Ackermann, H. Steinbusch, T. Vollmer, J. Wang, G. Jewell, and D. Howe, "A spherical permanent magnet actuator for a high-fidelity force-feedback joystick," *Mechatronics*, vol. 14, no. 3, pp. 327–339, Apr. 2004.
[28] J. Guo, C. Bak, and H. Son, "Design of a sensing system for a spherical motor based on Hall Effect sensors and neural networks," in *Proc. IEEE Int. Conf. Adv. Intell. Mechatronics (AIM)*, Jul. 2015, Art. no. 15403066.
[29] K. Bai and K.-M. Lee, "Direct field-feedback control of a ball-joint-like permanent-magnet spherical motor," *IEEE/ASME Trans. Mechatronics*, vol. 19, no. 3, pp. 975–986, Jun. 2014.
[30] J. Wang, G. Jewell, and D. Howe, "Analysis, design and control of a novel spherical permanent-magnet actuator," *IEE Proc.,-Electr. Power Appl.*, vol. 145, no. 1, p. 61, 1998.
[31] W. Wang, J. Wang, G. Jewell, and D. Howe, "Design and control of a novel spherical permanent magnet actuator with three degrees of freedom," *IEEE/ASME Trans. Mechatronics*, vol. 8, no. 4, pp. 457–468, Dec. 2003.
[32] H. Li and T. Li, "End-effect magnetic field analysis of the Halbach array permanent magnet spherical motor," *IEEE Trans. Magn.*, vol. 54, no. 4, Apr. 2018, Art. no. 8202209.
[33] C. Kian Lim, I.-M. Chen, L. Yan, G. Yang, and K.-M. Lee, "Electromechanical modeling of a permanent-magnet spherical actuator based on magnetic-dipole-moment principle," *IEEE Trans. Ind. Electron.*, vol. 56, no. 5, pp. 1640–1648, May 2009.
[34] H. Son and K.-M. Lee, "Distributed multipole models for design and control of PM actuators and sensors," *IEEE/ASME Trans. Mechatronics*, vol. 13, no. 2, pp. 228–238, Apr. 2008.
[35] H. Son, K.-M. Lee, J. Y. Song, and J. Park, "Effects of magnetic conducting boundary on design of electromagnetic actuators using image method," in *Proc. Int. Conf. Smart Manuf. Appl.*, Apr. 2008, pp. 172–177.
[36] W. Chen, L. Zhang, L. Yan, and J. Liu, "Design and control of a three degree of freedom permanent magnet spherical actuator," *Sens. Actuator A, Phys.*, vol. 180, pp. 75–86, Jun. 2012.
[37] J. Shen and S. Iwasaki, "Sensorless control of ultrahigh-speed PM brushless motor using PLL and third harmonic back EMF," *IEEE Trans. Ind. Electron.*, vol. 53, no. 2, pp. 421–428, Apr. 2006.
[38] Z. Chen, M. Tomita, S. Doki, and S. Okuma, "An extended electromotive force model for sensorless control of interior permanent-magnet synchronous motors," *IEEE Trans. Ind. Electron.*, vol. 50, no. 2, pp. 288–295, Apr. 2003.
[39] G. Schweitzer and E. Maslen, *Magnetic Bearings: Theory, Design, and Application to Rotating Machinery*. Berlin, Germany: Springer, 2009, ch. 16, pp. 461–485.
[40] L. Gan, Y. Pei, and F. Chai, "Tilting torque calculation of a novel tiered type permanent magnet spherical motor," *IEEE Trans. Ind. Electron.*, vol. 67, no. 1, pp. 421–431, Jan. 2020.
[41] F. Chai, L. Gan, and Y. Yu, "Magnetic field analysis of an iron-cored tiered type permanent magnet spherical motor using modified dynamic reluctance mesh method," *IEEE Trans. Ind. Electron.*, to be published, doi: 10.1109/tie.2019.2939964.

FENG CHAI (Member, IEEE) received the B.E. degree from Xi'an Jiaotong University, Xi'an, China, in 1994, and the M.E. and Ph.D. degrees from the Harbin Institute of Technology, Harbin, China, in 1998 and 2003, respectively, all in electrical engineering.

She is currently a Professor of electrical engineering with the Harbin Institute of Technology. She is involved in the design of permanent magnet machines and drives.

LEI GAN received the B.E. degree in electrical engineering from the Harbin Institute of Technology, Harbin, China, in 2014, where he is currently pursuing the Ph.D. degree in electrical engineering with the School of Electrical Engineering and Automation.

His current research interest includes electromagnetic design of multi-DOF actuators and permanent magnet synchronous machines.

LEI CHEN received the B.E., M.S., and Ph.D. degrees in electrical engineering from the Harbin Institute of Technology, Harbin, China, in 2004, 2006, and 2011, respectively.

He is currently an Associate Professor of electrical engineering with the Harbin Institute of Technology. His research interests include the design of novel electromagnetic device, and calculation of electromagnetic and temperature field in electric machines.